Principal components of dark energy with Supernova Legacy Survey supernovae: The effects of systematic errors

Eduardo J. Ruiz,[*] Daniel L. Shafer,[†] and Dragan Huterer[‡]

Department of Physics, University of Michigan, 450 Church Street, Ann Arbor, Michigan 48109-1040, USA

Alexander Conley[§]

Center for Astrophysics and Space Astronomy, University of Colorado, 389 UCB, Boulder, Colorado 80309-0389, USA

We study the effects of systematic errors in Type Ia supernova (SN Ia) measurements on dark energy (DE) constraints using current data from the Supernova Legacy Survey. We consider how SN systematic errors affect constraints from combined SN Ia, baryon acoustic oscillations, and cosmic microwave background data, given that SNe Ia still provide the strongest constraints on DE but are arguably subject to more significant systematics than the latter two probes. We focus our attention on the temporal evolution of DE described in terms of principal components (PCs) of the equation of state, though we examine a few of the more common, simpler parametrizations as well. We find that the SN Ia systematics degrade the total generalized figure of merit, which characterizes constraints in multidimensional DE parameter space, by a factor of 3 to 4. Nevertheless, overall constraints obtained on roughly five PCs are very good even with current data and systematics. We further show that current constraints are robust to allowing for the finite detection significance of the baryon acoustic oscillations feature in galaxy surveys.

PACS numbers: 95.36.+x, 98.80.−k

I. INTRODUCTION

Since the discovery of the accelerating universe in the late 1990s [1,2], a tremendous amount of effort has been devoted to improving measurements of dark energy (DE) parameters. As constraints on these parameters improved, controlling the systematic errors in measurements became critical for continued progress. The systematics come in many flavors, including a multitude of instrumental effects and astrophysical effects.

Type Ia supernovae (SNe Ia) were used to discover DE and still provide the best constraints on DE. The advantage of SNe Ia relative to other cosmological probes is that *every* supernova (SN) provides a distance measurement and therefore some information about DE. More recently, SN Ia observations have been joined by measurements of baryon acoustic oscillations (BAO), which provide exceedingly accurate measurements of the angular diameter distance in redshift bins. Cosmic microwave background (CMB) anisotropies come mostly from high redshift and are thus not particularly effective in probing DE, but they do provide one measurement of the angular diameter distance to redshift $z \simeq 1100$ very accurately. Galaxy clusters also constrain DE usefully, while weak gravitational lensing is expected to become one of the most effective probes of DE in the near future. For recent comprehensive reviews of DE probes, see Refs. [3,4].

In this work, we are interested in studying the effect of SN Ia systematics on DE constraints by including the *covariance* of measurements between different SNe. The covariance includes primarily systematic errors, and for the first time it has been quantified in depth by Conley *et al.* [5]. Including the effects of the systematic errors, represented by nonzero covariance, weakens the overall constraints on model parameters. Here we wish to explore the effect of systematic errors for general models of DE described by a number of principal components (PCs) of the equation of state, though we first consider these effects for simpler, more commonly used descriptions of the DE sector. We choose to combine the SN Ia data with BAO and CMB measurements and estimate the effects of *current* systematic errors in SN Ia observations. We then proceed to study another systematic concern that is particularly relevant for BAO: whether the finite significance of the detection of the BAO feature in various surveys, when taken into account, weakens the constraints imposed on DE parameters.

While we closely follow the accounting for the SN Ia systematics from Conley *et al.* [5], we note that several other analyses have considered the effect of SN systematics. However, most of these analyses only studied the effects of the systematic errors on the constant equation of state (e.g., Refs. [5–8]) or included the additional parameter w_a to describe the variation of the equation of state with time (e.g., Ref. [9]). Notable exceptions are studies by Davis *et al.* [10] and Rubin *et al.* [11], which considered a number of specific DE models with nonstandard behavior, and Amanullah *et al.* [12] and Suzuki *et al.* [13], which parametrized the DE density in several redshift bins. Here our goal is to go beyond any specific models and study the

[*]ejruiz@umich.edu
[†]dlshafer@umich.edu
[‡]huterer@umich.edu
[§]alexander.conley@colorado.edu

effects of systematic errors in current data on DE constraints in the greatest generality possible. While a truly model-independent description of the DE sector is of course impossible, a description of the expansion history in terms of ten or so parameters—which we adopt in this paper—comes close.[1] In this sense, our paper complements the recent investigations by Mortonson *et al.* [14,15] (see also Refs. [16–24]), which studied constraints on very general descriptions of DE using (a slightly different set of) current data but without specific study of the effects of systematic errors.

The paper is organized as follows. In Sec. II, we describe the SN Ia, BAO, and CMB data (and for BAO and CMB, the distilled observable quantities) that we use in our analysis. In Sec. III, we discuss useful parametrizations of DE and compare constraints on the DE parameters with and without systematic errors included in the analysis. In Sec. IV, we investigate the effects of the finite detection significance of the BAO feature in galaxy surveys on the cosmological parameter constraints. In Sec. V, we summarize our conclusions.

II. DATA SETS USED

We begin by describing the data sets used in this analysis. We have used three probes of DE: SNe Ia, BAO, and CMB anisotropies.

A. SN Ia data and covariance

Although SNe Ia are not, of course, perfect standard candles, it has long been known that there exist useful correlations between the peak apparent magnitude of a SN Ia and the *stretch*, or broadness, of its light curve (simply put, broader is brighter). The peak apparent magnitude is also correlated with the color of the light curve (bluer is brighter). We therefore model the apparent magnitude of a SN Ia with the equation [25]

$$m_{\text{mod}} = 5\log_{10}\left(\frac{H_0}{c}d_L\right) - \alpha_s(s-1) + \beta_c\mathcal{C} + \mathcal{M}, \quad (1)$$

where d_L is the luminosity distance, α_s is a nuisance parameter associated with the measured stretch s of a SN Ia light curve, and β_c is a nuisance parameter associated with the measured color $\mathcal{C}$ of the light curve. The absolute magnitude of a SN Ia is contained within the constant magnitude offset $\mathcal{M}$, which is considered yet another nuisance parameter.[2]

Recent work has concentrated on estimating correlations between measurements of individual SN Ia magnitudes. A complete covariance matrix for SNe Ia includes all identified sources of systematic error in addition to the intrinsic scatter and other sources of statistical error. The χ^2 statistic is then given by

$$\chi^2 = \Delta\mathbf{m}^T\mathbf{C}^{-1}\Delta\mathbf{m}, \quad (2)$$

where $\Delta\mathbf{m} = \mathbf{m}_{\text{obs}} - \mathbf{m}_{\text{mod}}(\mathbf{p})$ is the vector of magnitude differences between the observed magnitudes of N SNe Ia $\mathbf{m}_{\text{obs}}$ and the theoretical prediction that depends on the set of cosmological parameters $\mathbf{p}$, $\mathbf{m}_{\text{mod}}(\mathbf{p})$. Here $\mathbf{C}$ is the $N \times N$ covariance matrix between the SNe. Given a value for χ^2, we assume that the likelihood of a set of cosmological parameters is Gaussian, so that $\mathcal{L}(\mathbf{p}) \propto e^{-\chi^2/2}$. Since $\mathbf{C}$ is a function of parameters α_s and β_c (see below), we would naïvely expect that the inclusion of the Gaussian prefactor $1/\sqrt{\det\mathbf{C}}$ in the likelihood is necessary. However, using simple simulations of parameter extraction with synthetic data, we (and separately Conley *et al.* [5]) find that including the prefactor leads to significant *biases* in recovered α_s and β_c values. This result, discussed briefly in Ref. [5], is in hindsight not surprising given that both the independent variables (stretch and color) and dependent variable (magnitude) have errors; see e.g., Ref. [26] for a lengthy discussion. We therefore do not include the $1/\sqrt{\det\mathbf{C}}$ prefactor in our analysis.

Recently Conley *et al.* [5] determined covariances between SN Ia measurements from the Supernova Legacy Survey (SNLS). The SN compilation and covariance matrix that resulted from this work will be used in this analysis. The SNLS compilation consists of 472 SNe Ia, approximately one half of which were detected in SNLS, while the rest originated from one of three other sources. These four main sources are summarized in Table I and illustrated in the Hubble diagram of Fig. 1. The low-redshift (low-z) SNe actually come from a variety of samples as discussed in Conley *et al.* [5].

The complete covariance matrix from Ref. [5] can be written most usefully as the sum of two separate parts, a diagonal part consisting of typical statistical errors and a systematic part, which includes both diagonal and off-diagonal elements. This off-diagonal piece includes some correlated errors which are considered statistical in Ref. [5] (since they can be reduced by including more observations),

---

[1]We do not, however, consider allowing departures from general relativity; doing so would further generalize the treatment.

[2]Throughout the analyses in this paper, we actually marginalize analytically over a model with *two* distinct $\mathcal{M}$ values, where a mass cut of the host galaxy dictates which $\mathcal{M}$ value applies (here we use a mass cut of $10^{10}M_\odot$). This is meant to correct for host galaxy properties and is empirical in nature (see text and Appendix C of Ref. [5]). For simplicity, we suppress mention of the second $\mathcal{M}$ parameter.

TABLE I. Summary of SN Ia observations included in this analysis, showing the number of SNe included from each survey and the approximate redshift ranges.

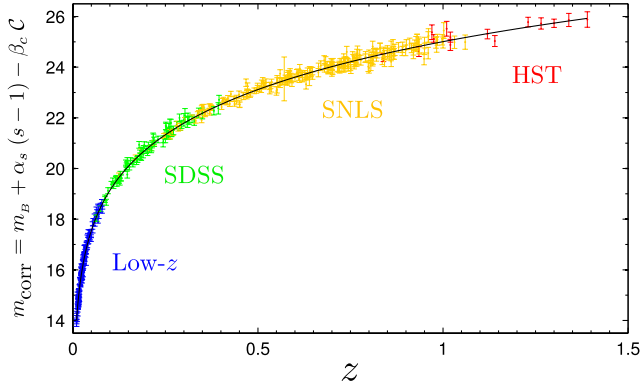| Source	N_{SN}	Range in z
Low z	123	0.01–0.1
SDSS	93	0.06–0.4
SNLS	242	0.08–1.05
HST	14	0.7–1.4

FIG. 1 (color online). Hubble diagram for the compilation of all SN Ia data used in this paper, labeling SNe from each survey separately and showing the (diagonal-only) magnitude uncertainties. The solid black line represents the best fit to the data.

but here we disregard the distinction and group these errors with the actual systematic errors, which also lead to off-diagonal covariance elements. This simplification is reasonable because the correlated statistical errors are small compared to the (correlated) systematic errors. The diagonal, statistical-only part of the covariance matrix can be expressed as

$$
\begin{aligned}
D_{ii}^{\text{stat}} = {}& \sigma_{m_B,i}^2 + \alpha_s^2 \sigma_{s,i}^2 + \beta_c^2 \sigma_{\mathcal{C},i}^2 + \sigma_{\text{int}}^2 \\
& + \left(\frac{5(1+z_i)}{z_i(1+z_i/2)\log 10} \right)^2 \sigma_{z,i}^2 + \sigma_{\text{lensing}}^2 \\
& + \sigma_{\text{host correction}}^2 + D_{ii}^{m_B s\mathcal{C}}(\alpha_s, \beta_c).
\end{aligned}
\tag{3}
$$

In the above, $\sigma_{m_B,i}$, $\sigma_{s,i}$, $\sigma_{\mathcal{C},i}$, and $\sigma_{z,i}$ are the statistical uncertainties of the measured magnitude, stretch, color, and redshift, respectively, of the ith SN. The z term translates the

error in redshift into error in magnitude. To include actual intrinsic scatter of SNe Ia and allow for any misestimates of photometric uncertainties, the quantity σ_{int} is included with a different value allowed for each sample. The σ_{int} values were derived by requiring the χ^2 of the best-fitting (Ω_M, w) cosmological fit to a flat universe to be 1 per degree of freedom for each sample separately. Also included here are statistical uncertainties due to gravitational lensing and uncertainty in the host galaxy correction.

The contribution $D_{ii}^{m_B s\mathcal{C}}(\alpha_s, \beta_c)$ represents a combination of the covariance terms between magnitude, stretch, and color for the ith SN. It is given by

$$
D_{ii}^{m_B s\mathcal{C}}(\alpha_s, \beta_c) = 2\alpha_s D_{ii}^{m_B s} - 2\beta_c D_{ii}^{m_B \mathcal{C}} - 2\alpha_s \beta_c D_{ii}^{s\mathcal{C}}, \tag{4}
$$

where $D_{ii}^{m_B s}$, $D_{ii}^{m_B \mathcal{C}}$, and $D_{ii}^{s\mathcal{C}}$ represent the computed magnitude-stretch, magnitude-color, and stretch-color covariances for the ith SN. Note that even the statistical covariance matrix is a function of α_s and β_c, meaning that a proper analysis involves varying the errors (recomputing the covariance matrix) any time α_s and β_c are changed.

A similar equation can be used to construct the systematic covariance matrix, where different systematic terms are combined to produce submatrices which are then added together with specified values for α_s and β_c, as above. The systematic terms include calibration (which is the dominant contribution), Malmquist bias, peculiar velocities, Milky Way dust extinction, contamination of the sample with non-Ia SNe, uncertainties arising from differences in the light-curve fitters, uncertainty in the relationship between host galaxy properties and SN magnitude, evolution of α_s and β_c, and early light-curve photometric uncertainty. The systematic covariance matrix includes
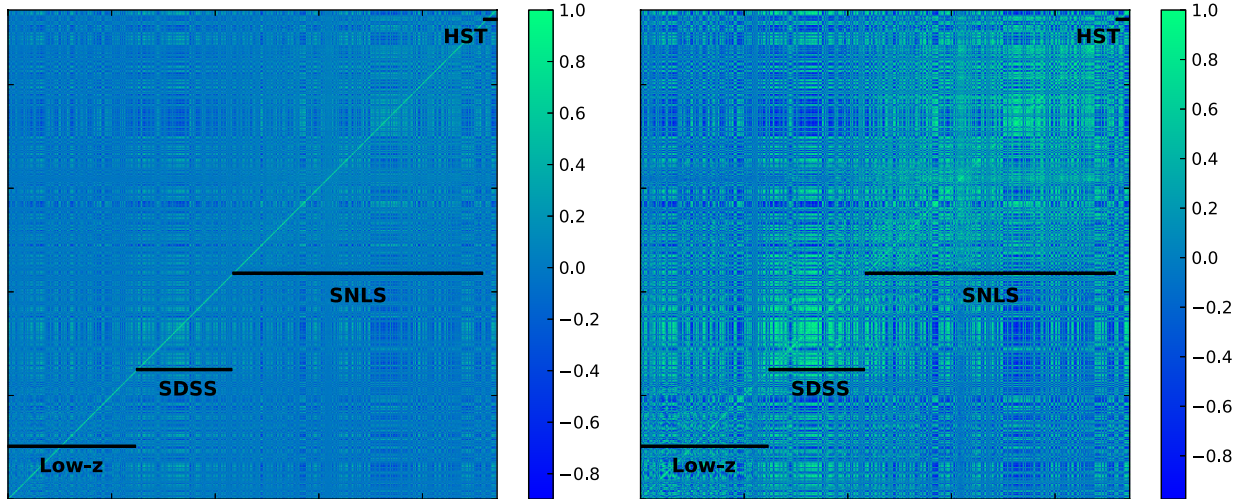

FIG. 2 (color online). Left panel: correlation matrix obtained from the complete covariance matrix $\mathbf{C}^{\text{full}}$, sorted first by survey and then by redshift within each survey. Right panel: same, but using only the systematic covariance matrix $\mathbf{C}^{\text{sys}}$. In both cases we assume $\alpha_s = 1.43$ and $\beta_c = 3.26$, the best-fit values for the flat $w = \text{const}$ model. The right panel is similar to Fig. 12 from Ref. [5], but we repeat it here and show the full covariance (left panel) for completeness.

diagonal and off-diagonal elements, which are calculated (see Ref. [5] for more details) using the equation

$$C_{ij}^{\text{sys}} = \sum_{k=1}^{K} \left(\frac{\partial m_{\text{mod}i}}{\partial S_k}\right)\left(\frac{\partial m_{\text{mod}j}}{\partial S_k}\right)(\Delta S_k)^2, \qquad (5)$$

where the sum is over the K systematics S_k, ΔS_k is the size of each term (for example, the uncertainty in the zero point), and m_{mod} is defined in Eq. (1). Then the full covariance matrix is simply given by

$$\mathbf{C}^{\text{full}} = \mathbf{D}^{\text{stat}} + \mathbf{C}^{\text{sys}}. \qquad (6)$$

A plot of the full covariance matrix (constructed using flat $w = \text{const}$ model best-fit values $\alpha_s = 1.43$ and $\beta_c = 3.26$) is shown in Fig. 2.

B. BAO and CMB data

To produce the combined constraints in this paper, we include information from both BAO and the CMB in addition to the SN data. In each case, we choose for simplicity distilled quantities which depend only on Ω_M, Ω_{DE}, Ω_K, and a parametrized $w(z)$.

For BAO, we compare the theoretical prediction for the acoustic parameter $A(z)$ with the measured value, where we define (see Eisenstein *et al.* [27])

$$A(z) \equiv \left[r^2(z)\frac{cz}{H(z)}\right]^{1/3}\frac{\sqrt{\Omega_M H_0^2}}{cz}, \qquad (7)$$

where $r(z)$ is the comoving distance to redshift z. We combine recent measurements of $A(z)$ at different effective redshifts, using data from the 6dF Galaxy Survey [28], the Sloan Digital Sky Survey (SDSS) Data Release 7 (DR7) [29], the WiggleZ survey [30,31], and the SDSS Baryon Oscillation Spectroscopic Survey (BOSS) [32,33]. The measured values are summarized in Table II.

A plot of the measured values and their uncertainties superimposed on an $A(z)$ curve (Fig. 3) suggests that there is no significant tension between the measurements. Note that the SDSS DR7 measurements at $z = (0.2, 0.35)$ are correlated with correlation coefficient 0.337. The WiggleZ

TABLE II. Summary of measurements of distilled BAO parameter $A(z)$. We show the survey from which the measurement comes, the effective redshift of the survey (or its subsample), and the measured value A_0.

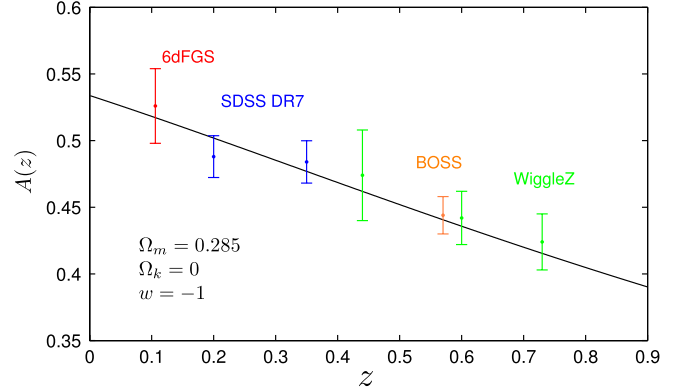| Sample	z_{eff}	$A_0(z_{\text{eff}})$
6dFGS	0.106	0.526 ± 0.028
SDSS DR7	0.20	0.488 ± 0.016
SDSS DR7	0.35	0.484 ± 0.016
WiggleZ	0.44	0.474 ± 0.034
BOSS	0.57	0.444 ± 0.014
WiggleZ	0.60	0.442 ± 0.020
WiggleZ	0.73	0.424 ± 0.021

FIG. 3 (color online). Measured values of $A(z)$ and their (diagonal-only) uncertainties for each effective redshift. The black curve shows $A(z)$ for a model that fits the data points well, and the parameters for this model are given in the legend.

measurements are correlated with coefficient 0.369 for the pair $z = (0.44, 0.6)$ and coefficient 0.438 for $z = (0.6, 0.73)$. Ignoring the relatively small overlap in survey volume between SDSS DR7 and the BOSS sample, we expect all other pairwise correlations to be zero. We compute χ^2 in the usual way for correlated measurements, as in Eq. (2).

Nearly all of the sensitivity of the CMB to DE comes from the measurement of an angle at which the sound horizon at $z \approx 1100$ is observed (e.g., Ref. [34]). This measurement in turn determines the angular diameter distance to recombination with the physical matter quantity, $\Omega_M h^2$, essentially fixed. The latter quantity is popularly known as the CMB shift parameter R and is defined as

$$R \equiv \frac{\sqrt{\Omega_M H_0^2}}{c} r(z_*), \qquad (8)$$

where $z_* = 1091.3$ is the redshift of decoupling as measured by WMAP7 [35]. We take the measured value of R to be the value determined by WMAP7, $R_0 = 1.725 \pm 0.0184$ [35]. We compute χ^2 in the usual way, comparing this measured value of R with the theoretical prediction.

Calculating the combined SN, BAO, and CMB likelihood is now a simple task. We define $\mathcal{L}_{\text{comb}} \propto e^{-\chi_{\text{tot}}^2/2}$, where $\chi_{\text{tot}}^2 = \chi_{\text{SN}}^2 + \chi_{\text{BAO}}^2 + \chi_{\text{CMB}}^2$.

C. Parameter constraint methodology

We use two alternate codes to produce our constraints. For the basic constraints, including the constant equation of state of DE or the (w_0, w_a) description, we use a brute-force search which computes likelihoods over a grid of values of ~ 5 parameters (listed below).

Alternatively, we developed a new Markov Chain Monte Carlo (MCMC; e.g., see Refs. [36,37]) code to determine DE parameter constraints and figures of merit (FoMs) for the general (~ 13 parameters) PC description. The MCMC procedure is based on the Metropolis-Hastings

algorithm [38,39]. From the likelihood $\mathcal{L}(\mathbf{x}|\theta)$ of the data $\mathbf{x}$ given each proposed parameter set θ, Bayes' theorem tells us that the posterior probability distribution of the parameter set given the data is

$$\mathcal{P}(\theta|\mathbf{x}) = \frac{\mathcal{L}(\mathbf{x}|\theta)\mathcal{P}(\theta)}{\int \mathcal{L}(\mathbf{x}|\theta)\mathcal{P}(\theta)d\theta}, \qquad (9)$$

where $\mathcal{P}(\theta)$ is the prior probability density. The MCMC algorithm generates random draws from the posterior distribution. We test convergence of the samples to a stationary distribution that approximates $\mathcal{P}(\theta|\mathbf{x})$ by applying a conservative Gelman-Rubin criterion [40] of $R - 1 \lesssim 0.03$ across a minimum of four chains for each model class. We use the GETDIST routine of the CosmoMC code [41,42] to process the resulting chains; GETDIST bins the chains and then smoothes the binned distribution of counts by convolution with a multidimensional Gaussian kernel.

We verified that the two codes give results that are in excellent agreement in several relevant cases, e.g., constraints in the Ω_M-w or w_0-w_a plane.

III. RESULTS: EFFECTS OF THE SYSTEMATICS

A. Preliminaries

Before beginning our discussion of systematics, we briefly consider the vanilla ΛCDM cosmology, where $w = -1$. The cosmological parameters describing the expansion rate are matter and cosmological constant densities relative to critical Ω_M and Ω_Λ. Including the nuisance parameters, the total parameter set is

$$p_i \in \{\Omega_M, \Omega_\Lambda, \mathcal{M}, \alpha_s, \beta_c\}. \qquad (10)$$

We combine SN constraints with BAO and CMB constraints and marginalize over the other parameters to map the likelihood of Ω_Λ. We find a mean value $\Omega_\Lambda = 0.724 \pm 0.0114$. This suggests that a universe with zero (or negative) cosmological constant is ruled out at approximately 64-σ. Amusingly, using the brute-force likelihood search that includes the positive and negative values of Ω_Λ, we find that the combined data give a remarkably low likelihood of zero or negative vacuum energy, even allowing for nonzero curvature: $P(\Omega_\Lambda \leq 0) \sim 10^{-267}$. Of course, in reality, the evidence for DE is not nearly this convincing, since the likelihood in the space of cosmological observables is certainly not expected to be Gaussian this far away from the peak and thus would *not* be described by $\mathcal{L}_{\text{comb}} \propto e^{-\chi^2_{\text{tot}}/2}$ (we discuss a related issue in Sec. IV). Nonetheless, it is impressive how strong the evidence for DE is with current data.

We now discuss how one goes beyond ΛCDM cosmology by parametrizing the DE equation of state.

Previous work on the effect of systematics, such as Ref. [5], considered the DE sector parametrized by its energy density relative to critical Ω_{DE} and a constant equation of state w. Here, we are particularly interested in extending the DE sector to allow for a time-varying

equation of state. We make two alternative choices in addition to the constant equation of state so that the three parametrizations we consider are

(1) Constant equation of state, $w = $ constant,
(2) Equation of state described with w_0 and w_a [43], so that $w(a) = w_0 + w_a(1 - a)$,
(3) Equation of state described by a finite number of principal components of $w(z)$ [44].

We now describe in more detail the different parametrizations of DE that we consider (constant w, w_0, and w_a, PCs) and then proceed to analyze the effects of SN systematics on parameter constraints.

B. Constant w

Assuming that DE can be described by an equation of state w that is constant in time, and assuming a flat universe, we calculate the SN-only likelihood in the Ω_M-w plane. We marginalize over the usual nuisance parameters $\mathcal{M}$, α_s, and β_c.

The results for SN-only constraints on Ω_M and w are shown in Fig. 4, where we illustrate the effect of the systematics by showing constraints from the full covariance matrix $\mathbf{C}^{\text{full}}$ on top of those which assume only the diagonal statistical uncertainties $\mathbf{D}^{\text{stat}}$. The systematic uncertainties broaden the well-determined direction in the Ω_M-w plane without elongating the poorly determined direction much. Constraints in either parameter are not appreciably shifted. The marginalized uncertainty for w is $\sigma_w = 0.17$ for statistical errors only and $\sigma_w = 0.20$ when systematic errors are included. Thus, even though systematic errors increase the area of the contours in the Ω_M-w plane by more than a factor of 2, they only increase the uncertainty of w by about 20%.

We also seek to understand how SN systematics influence the stretch and color parameters α_s and β_c, not only
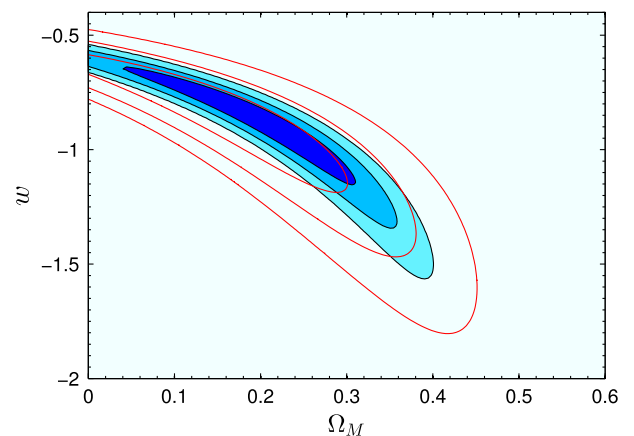

FIG. 4 (color online). The 68.3%, 95.4%, and 99.7% likelihood constraints on Ω_M and w, assuming a constant value for w and a flat universe. We use only SN data and marginalize over the nuisance parameters. We compare the case of diagonal statistical errors only (shaded blue) with the full covariance matrix (red).
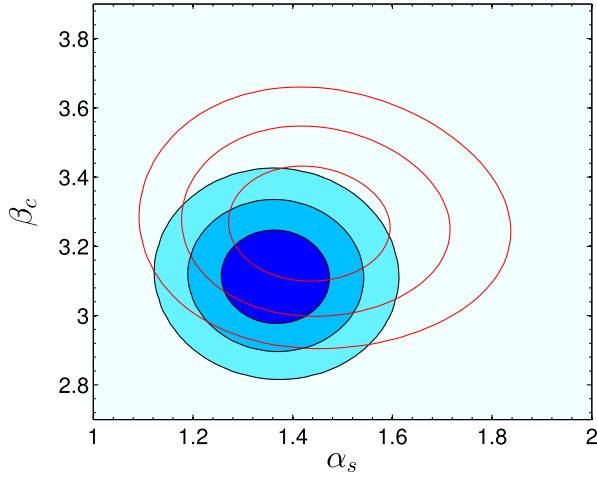
FIG. 5 (color online). The 68.3%, 95.4%, and 99.7% likelihood constraints on α_s and β_c, assuming a constant value for w and a flat universe. We use only SN data and marginalize over $\mathcal{M}$, Ω_M, and w. We compare the case of diagonal statistical errors only (shaded blue) with the full covariance matrix (red).

because these correlations are what make SNe Ia useful standard candles, but also because it is expected that systematics could potentially affect these correlations. In Fig. 5, we marginalize over $\mathcal{M}$, Ω_M, and w to show constraints on the stretch and color coefficients α_s and β_c. Of particular interest is the color coefficient β_c, which is broadly consistent with values found previously; the

systematic errors shift it slightly upwards and increase errors in both parameters by a modest amount.

C. w_0 and w_a

We wish to understand the constraints on the redshift dependence of $w(z)$, so we allow $w(z)$ to have the form [43,45]

$$w(z) = w_0 + w_a z/(1+z). \tag{11}$$

Constraints on w_0 and w_a in a flat universe are shown in Fig. 6. The shaded blue contours represent constraints with only statistical SN errors assumed ($\mathbf{D}^{\text{stat}}$), while the red contours ($\mathbf{C}^{\text{full}}$) additionally include the systematic errors. The left panel shows SN-only constraints, while the right panel shows constraints when BAO and CMB information is also included.

The figure of merit (FoM) for this model defined by the Dark Energy Task Force (DETF) [46,47] is the inverse of the area of the 95.4% confidence level region A_{95} in the w_0-w_a plane; to be slightly more specific, we instead define the FoM as in Mortonson *et al.* [15] as

$$\text{FoM}^{(w_0 w_a)} \equiv (\det \mathbf{C})^{-1/2} \approx \frac{6.17\pi}{A_{95}}. \tag{12}$$

The approximate equality in Eq. (12) becomes exact for a Gaussian posterior distribution, in which case our FoM is equivalent to the DETF FoM. The FoMs for various scenarios in the w_0-w_a plane are given in Table III. We find
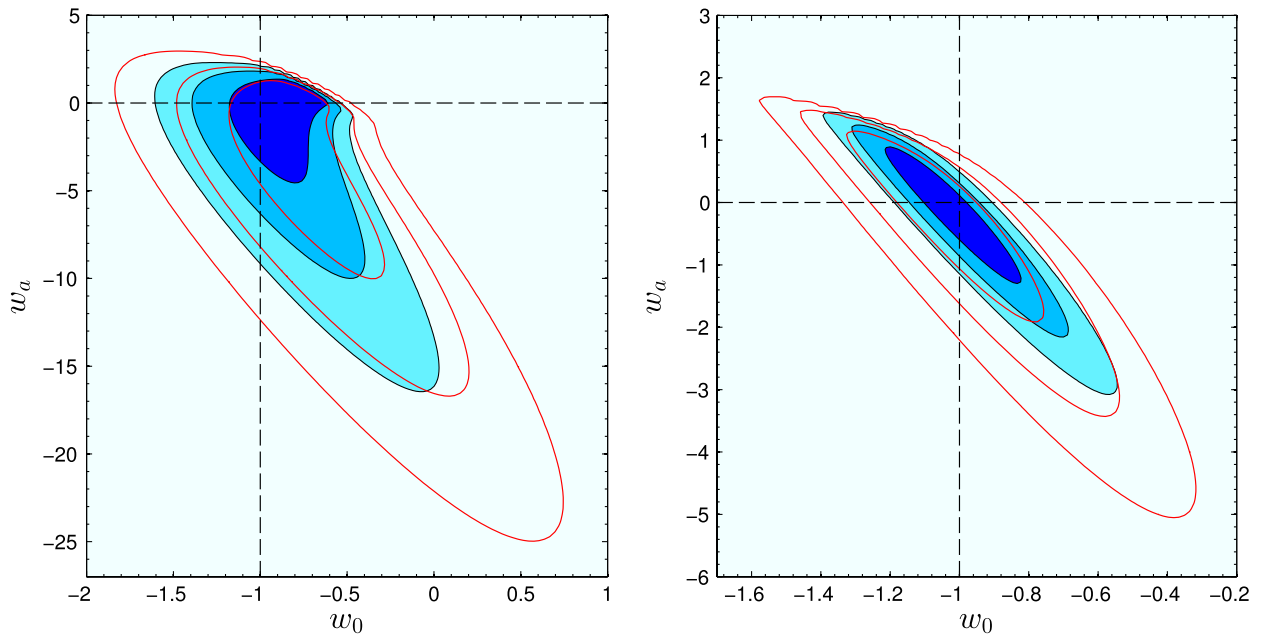

FIG. 6 (color online). The 68.3%, 95.4%, and 99.7% likelihood constraints on w_0 and w_a in a flat universe, marginalized over Ω_M and the nuisance parameters. The left panel shows SN-only constraints, while the right panel shows combined SN + BAO + CMB constraints. The shaded blue contours represent constraints with only statistical SN errors assumed ($\mathbf{D}^{\text{stat}}$), while the red contours represent the full SN covariance matrix ($\mathbf{C}^{\text{full}}$). Note that the ΛCDM model $(w_0, w_a) = (-1, 0)$, represented by the black dashed lines, is fully consistent with the data.

TABLE III. Values of the FoM [Eq. (12)] for SN alone (middle row) and SN + BAO + CMB (bottom row). The middle column shows the FoMs for the statistical covariance matrix $\mathbf{D}^{\text{stat}}$ only, while the right column shows the FoMs for the full covariance matrix $\mathbf{C}^{\text{full}}$. Note that including the systematics reduces the FoM by a factor of 2 to 3.

$\text{FoM}^{(w_0 w_a)}$	$\mathbf{D}^{\text{stat}}$	$\mathbf{C}^{\text{full}}$
SN	2.28	1.16
SN + BAO + CMB	32.9	11.8

that including the systematic errors reduces the FoM by about a factor of 2 to 3.

D. Principal components

We now describe the methodology of how to calculate and constrain the principal components of DE [44], which are weights in redshift ordered by how well they are measured by a given cosmological probe and with a given survey.

Following e.g., Mortonson et al. [14], we first precompute the PCs assuming the current data *centered at a fixed fiducial model* (we choose the standard flat ΛCDM model with $\Omega_M = 1 - \Omega_\Lambda = 0.25$). For this precomputation, we include data from all probes (SN + BAO + CMB) and use all identified SN errors. We follow the procedure set forth by the Figure of Merit Science Working Group (FoMSWG) [48] and parametrize $w(z)$ by 36 piecewise constant values in bins uniformly spaced in scale factor a in the range $0.1 \leq a \leq 1.0$. We fix (i.e., ignore) all other parameters in the FoMSWG except for Ω_M and the SN Ia nuisance parameter[3] $\mathcal{M}$ because they are not probed by the SN Ia data, and at the same time they are effectively marginalized over in the BAO and CMB data in the distilled observable quantities $A(z)$ and R, respectively. We fix curvature to zero.

We therefore have a 38×38 Fisher matrix (or really a 45×45 Fisher matrix with seven parameters fixed), corresponding to parameters

$$p_i \in \{w_1, \ldots, w_{36}, \Omega_M, \mathcal{M}\}. \tag{13}$$

We marginalize over Ω_M and $\mathcal{M}$ and then diagonalize the remaining 36-dimensional Fisher matrix of the piecewise constant w parameters. The resulting eigenvectors—shapes that describe $w(z)$—are the PCs $e_i(z)$, and we show the ten best determined of these PCs, $e_1(z)$–$e_{10}(z)$, in Fig. 7.

---

[3]In the Fisher matrix precomputation of the PCs we assume a single $\mathcal{M}$ parameter as per usual practice (and following the FoMSWG parametrization), but in the actual constraints on the cosmological parameters we adopt *two* such parameters as described in Sec. II A. To the extent that the PCs will be correlated anyway due to the differences between real data and assumed ''data'' going into the Fisher matrix, this subtle difference will be unimportant.
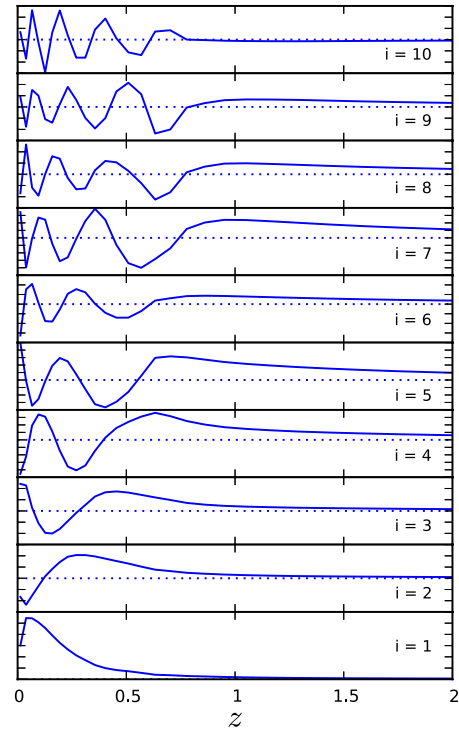

FIG. 7 (color online). The first ten PCs, $e_1(z)$–$e_{10}(z)$, used in our analysis, in order of increasing variance (bottom to top). The PCs were obtained assuming the observable quantities centered at the fiducial ΛCDM model, but with actual errors from the current data. See text for details.

The equation of state can be described as [49]

$$1 + w(z) = \sum_{i=1}^{N} \alpha_i e_i(z), \tag{14}$$

where α_i are amplitudes for each PC $e_i(z)$. While the Fisher matrix tells us the best accuracy to which these PCs are measured using the assumed data set [these accuracies are related to the eigenvalues λ_i via $\sigma(\alpha_i) = \lambda_i^{-1/2}$], we are not interested in this; rather, we would like to constrain the PCs using actual current data.

We then feed the shapes in redshift of the first several PCs to the MCMC procedure to constrain these [and a few other non-$w(z)$] parameters.

Finally, in our parameter search we impose weak priors on the PCs. Following Ref. [49] we impose a hard-bound prior on each α_i, enforcing its contribution to excursions in the equation of state to the region $|1 + w(z)| \leq 1$. This approach yields top-hat priors of width [15]

$$\Delta \alpha_i = \frac{2}{N_{z,\text{PC}}} \sum_{j=1}^{N_{z,\text{PC}}} |e_i(z_j)| \tag{15}$$

centered at $w(z) = -1$ or $\alpha_i = 0$. As we will demonstrate, these priors are much wider than the allowed ranges for many of the individual PCs, meaning that our principal
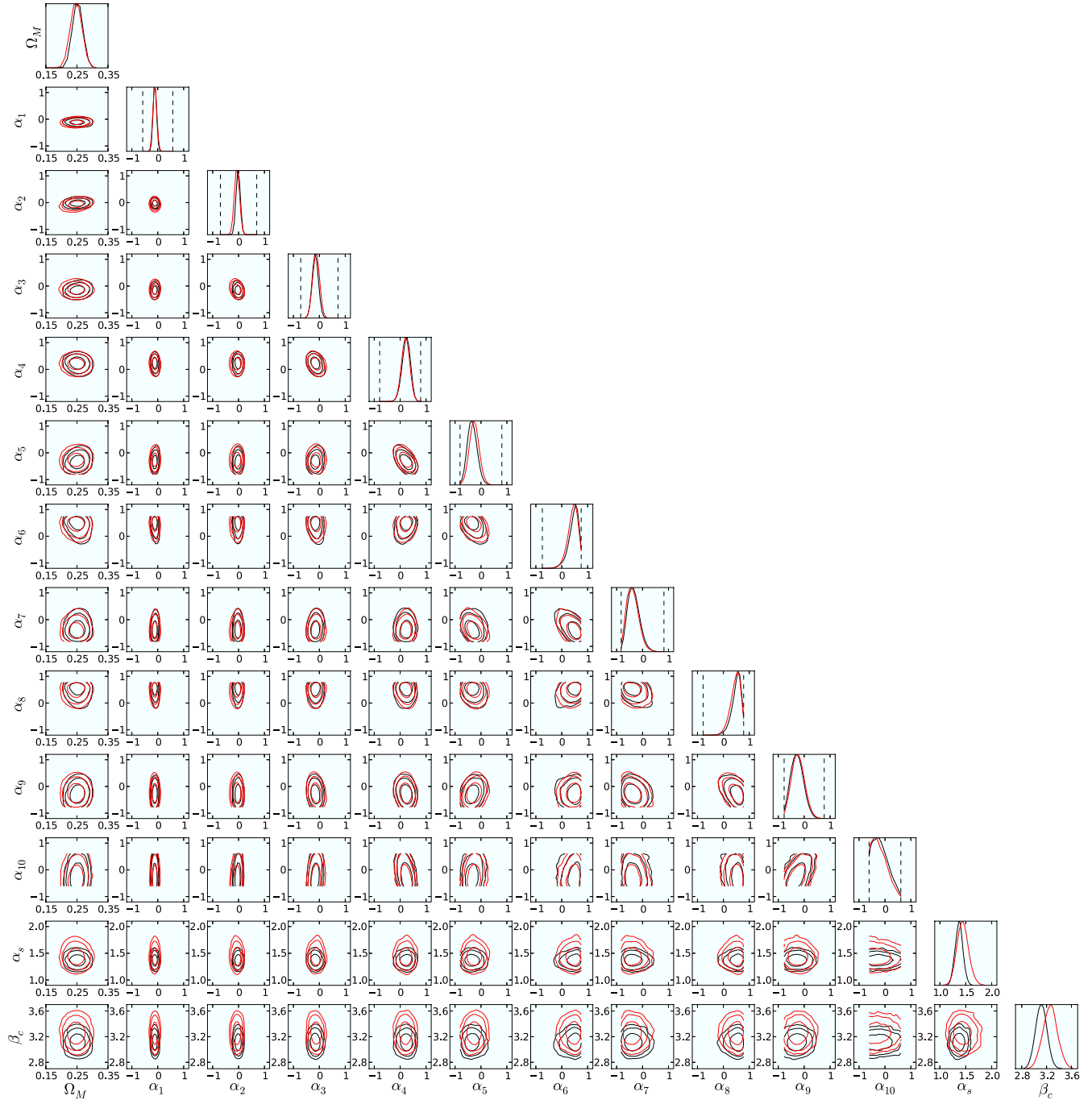
FIG. 8 (color online). The 68.3%, 95.4%, and 99.7% likelihood constraints for all pairwise combinations of the 13 cosmological parameters using the combined SN + BAO + CMB data. Diagonal boxes show the 1D marginalized likelihood for each parameter. The black contours illustrate the case of diagonal statistical SN errors only ($\mathbf{D}^{\text{stat}}$), while the red contours ($\mathbf{C}^{\text{full}}$) also include the systematic SN covariance matrix. The parameter ordering is (top to bottom, or left to right) as follows: matter density relative to critical Ω_M, the ten PC amplitudes α_1–α_{10}, and the stretch and color nuisance parameters α_s and β_c. Note the good constraints on all parameters except for the last few PC amplitudes.

results are largely unaffected by the prior (indeed, we verified this explicitly by constraining the PCs without the prior).

The pairwise constraints on all 13 parameters (Ω_M, the PC amplitudes α_1–α_{10}, and the nuisance parameters α_s and β_c) are shown in Fig. 8. The black curves represent constraints from the diagonal statistical SN errors only, while the red curves correspond to the full SN covariance matrix. Overall, the systematic errors broaden and shift the contours slightly.
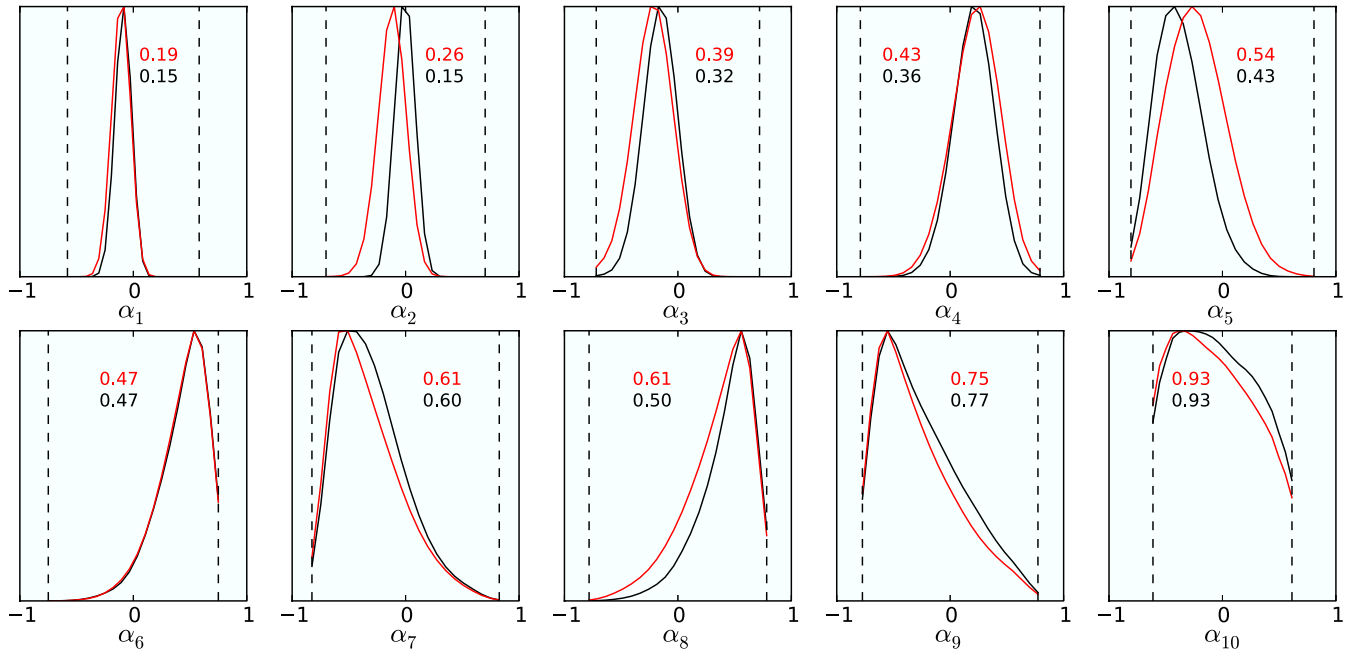
FIG. 9 (color online).   Marginalized SN + BAO + CMB constraints on the ten PC amplitudes. The dashed vertical lines represent the prior limits. Black curves represent constraints from the diagonal statistical SN errors only, while the red curves correspond to the full SN covariance matrix. The black and red number in each panel shows the ratio of the PC error to the rms of the top-hat prior for the statistical-covariance and full-covariance cases, respectively. Note the good constraints on all PC amplitudes except for the last few.

In Fig. 9, we show the individual marginalized constraints on the ten PC amplitudes. When we assume only diagonal statistical errors, three PCs have a ratio of error to the rms value of the top-hat prior less than $1/3$, and six PCs have a ratio less than $1/2$. For the full covariance case, two and five PCs have error/prior ratios less than $1/3$ and $1/2$, respectively. From this, we are extremely encouraged by the fact that constraints on several PCs are very good even with current data, a result incidentally also found by Ref. [14] using a slightly different combined ''current'' data set that most notably did not include the BOSS and WiggleZ BAO measurements. Here we again see that the SN systematics broaden the constraints slightly; however, as we show just below, the cumulative effect of the systematics on the FoM is not negligible.

We finally calculate the generalization of the DETF FoM to PCs. As defined in Mortonson *et al.* [15],

$$\mathrm{FoM}_n^{(PC)} \equiv \left(\frac{\det \mathbf{C}_n}{\det \mathbf{C}_n^{(\mathrm{prior})}}\right)^{-1/2}, \qquad (16)$$

where $\mathbf{C}_n$ is the $n \times n$ covariance submatrix of n PCs and

$$\det \mathbf{C}_n^{(\mathrm{prior})} = \prod_{i=1}^{n} \left(\frac{\Delta \alpha_i}{\sqrt{12}}\right)^2$$

is the determinant of the top-hat prior covariance for the n PC coefficients. Each $(\Delta \alpha_i / \sqrt{12})^2$ term refers to the rms value of the top-hat prior, where $\Delta \alpha_i$ is the width of the top-hat prior as calculated in Eq. (15).

FoM results are shown in Fig. 10, where we show the FoM as a function of the number of PCs included. The top panel shows the FoMs with and without SN systematic errors, while the bottom panel shows the corresponding ratios of the two cases. We see that the FoM degradation with the addition of SN systematic errors asymptotes to about a factor of 3 to 4 when about five PCs are included and after that remains relatively constant. We therefore conclude that only the few lowest PCs are affected by current systematic errors. We suspect that this is due to the fact that the effect of the systematics is relatively smooth in redshift, and therefore systematics do not become degenerate with the higher PCs that wiggle in z (see the PC shapes in Fig. 7). It is somewhat fortuitous that higher ($n \gtrsim 5$) PCs seem to be unaffected by systematics, since it is precisely those higher PCs that are difficult to measure accurately; however, it may be the case that systematics in future data will behave differently and affect the higher components.

IV. EFFECT OF FINITE DETECTION SIGNIFICANCE OF BAO

In an interesting paper, Bassett and Afshordi [50] pointed out that for marginal detections of cosmological observable quantities, a Gaussian assumption for the likelihood may be a poor one, especially for models that are several σ away from the central value of the observed quantity. This happens because the usual Gaussian likelihood implicitly ignores the possibility that the observed
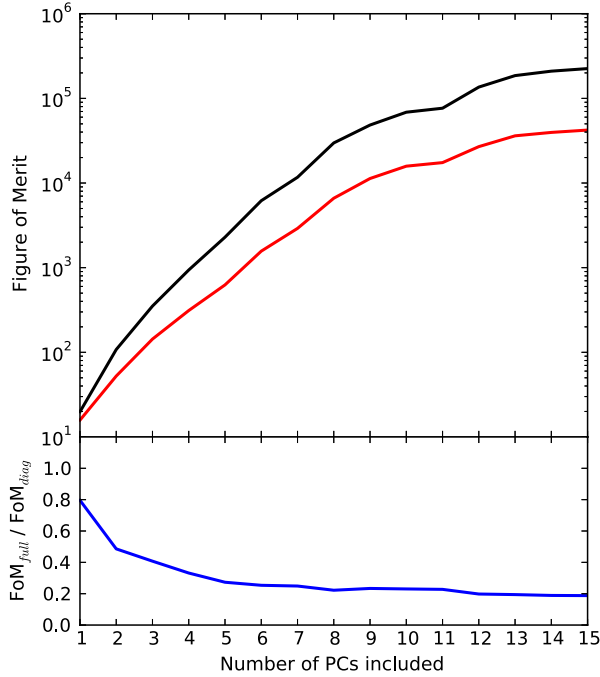
FIG. 10 (color online). Top panel: FoM as a function of the number of PCs included, with the black line showing the statistical-only FoM and the red line showing the FoM with systematics included [see Eq. (16) for the definition of the FoM]. Bottom panel: ratio of the FoM with systematic errors considered in the SN Ia data to that with only statistical errors considered. BAO and CMB constraints were included in both cases. Notice that the FoM ratio levels off after approximately five PCs have been included. Note that here we have considered the first 15 PCs (as opposed to ten in Figs. 7–9) to show that the FoM indeed flattens off as the PCs become very poorly constrained.

quantity has *not* actually been detected in the data at all. That possibility may have non-negligible probability, and in that case a flat likelihood in the observable may be more appropriate. In other words, writing a total likelihood of parameters **p** as a function of data vector **d**, we have

$$P(\mathbf{p}|\mathbf{d}) = P_{\text{detect}} P(\mathbf{p}|\mathbf{d}, \text{detect})$$
$$+ (1 - P_{\text{detect}}) P(\mathbf{p}|\mathbf{d}, \text{noise}),$$

where P_{detect} is the probability that the observable quantity has actually been detected and $P(\mathbf{p}|\mathbf{d}, \text{detect})$ is the likelihood of the cosmological parameters in that case. The cosmological parameter likelihood $P(\mathbf{p}|\mathbf{d}, \text{noise})$ corresponds to the case that the observable feature was actually noise, and it can be represented by a flat distribution in the parameters **p**. *Most BAO analyses effectively assume that* $P_{\text{detect}} = 1$, thus ignoring the higher-than-expected tail in the overall likelihood coming from the nonzero second term on the right-hand side of Eq. (17). If the BAO feature has been detected at very high significance, then this is a

good assumption, but it is not *a priori* clear that this is the case with all of the current BAO surveys which typically have several σ detection significances.

To account for the diminished power of the observations to discriminate between cosmological models when detection significance is not high, Bassett and Afshordi [50] suggest a fitting function which replaces the usual Gaussian χ^2 expression $\Delta\chi_G^2$ with

$$\chi^2 = \frac{\Delta\chi_G^2}{\sqrt{1 + (\frac{S}{N})^{-4}\Delta\chi_G^4}}, \qquad (18)$$

where S/N is the signal-to-noise ratio or detection significance of the observable feature or quantity. With this prescription, the quantity $\Delta\chi^2$ is equal to its Gaussian counterpart for departures from the best-fit model that are small compared to the signal-to-noise of the observed feature, but it asymptotes to a constant "tail" $(S/N)^2$ in the opposite limit, when $\Delta\chi_G^2 \gg (S/N)^2$.

Here we apply this reasoning to the measurement of the BAO feature. The significances of the detection of the BAO feature are 2.4σ (corresponding to S/N = 2.4) for 6dF [28], 2.8σ for WiggleZ [31] (combined for three redshift bins), 3.6σ for SDSS [29] (combined for two redshift bins), and 5.0σ for BOSS [33]. We expect that once the probability of nondetection of the BAO feature has been included, the BAO constraints will change, especially for surveys with lower significance of detection and for 99.7% contour regions. This has in fact been confirmed by Bassett and Afshordi [50] for the case of the SDSS BAO data alone.

Figure 11 shows the BAO-only (left panel) and BAO + CMB + SN (right panel) constraints in the Ω_M-w plane with and without the finite detection of the BAO features taken into account.[4] Note that the difference is modest in the BAO-only case and negligible in the combined case. This is as expected, especially given that some of the strongest BAO data sets (e.g., BOSS) also have the highest detection significances of the BAO feature.

Note also that there is nothing BAO specific to the effects of the finite detection significance. While the CMB is detected with very high confidence and thus does not warrant a similar analysis, it could be applied to SNe Ia where, for example, a few percent of SNe may not be Type Ia.[5] Given the full probabilistic classification of each SN on whether or not it is Type Ia [51,52], one could carry out a similar analysis, which in this context would be how imperfect purity of the SN Ia sample affects the constraints on cosmological parameters. We suspect the

---

[4]The results in the w_0-w_a plane are qualitatively similar, and we do not show them here.
[5]Conley *et al.* [5] find that the fraction of non-Ia SNe rises from zero at low redshift to $O(10\%)$ at $z \sim 1$; however, their modeling is very conservative, and the true fraction of non-Ia SNe is likely very small in the current data sets.
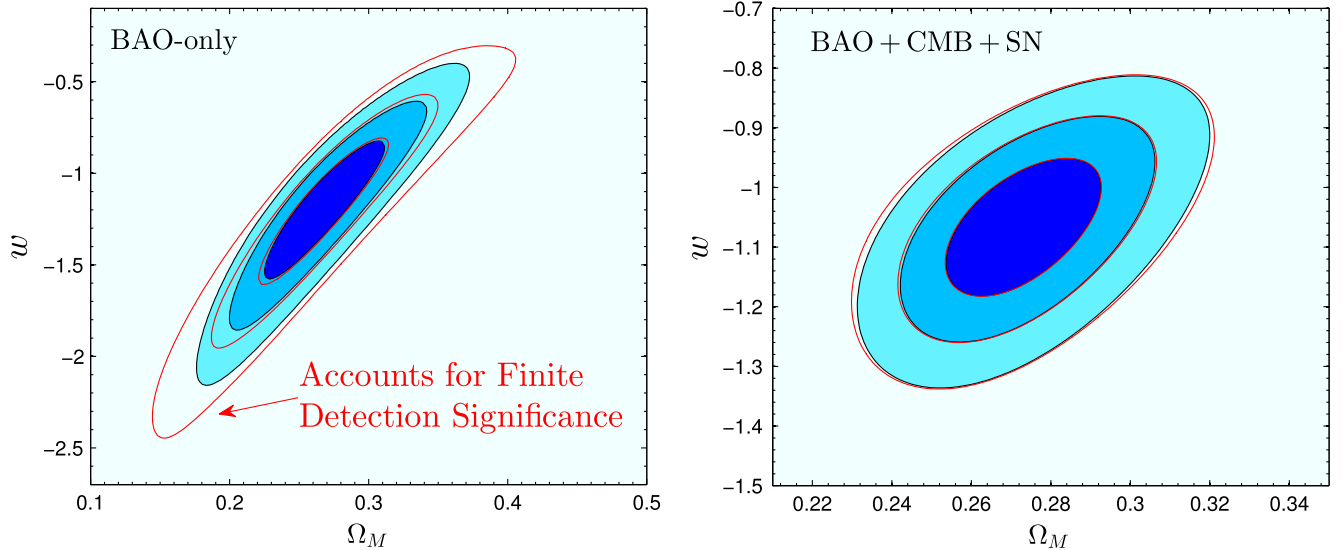
FIG. 11 (color online). Effects on the BAO-only (left panel) and BAO + CMB + SN (right panel) constraints in the Ω_M-w plane with (red) and without (shaded blue) the finite detection significances of the BAO features taken into account. Note that the differences are modest in the BAO-only case and negligible in the combined case.

results would be even less discrepant relative to the usual perfect-detection analysis than in the case of BAO, and we do not pursue such an analysis in this paper.

In conclusion, the finite detection significance of the BAO feature in large-scale structure surveys leads to a small but discernible weakening of the constraints on cosmological parameters.

V. CONCLUSIONS

In this paper, we have investigated the effects of systematic errors in current SN Ia observations on DE parameter constraints. We accounted for the systematic errors in SN Ia observations, including the effects of photometric calibration, dust, color, gravitational lensing, and other systematics by adopting a fully off-diagonal covariance matrix between ~500 SNe from the SNLS compilation (see Fig. 2). We extended the similar analysis from Conley *et al.* [5] by constraining the temporal evolution of the equation of state of DE described by the pair of parameters (w_0, w_a) as well as a much richer description in terms of ten PCs of the equation of state (shown in Fig. 7). We combined the SN Ia constraints with data from BAO from four different surveys (see Fig. 3) as well as the principal information on DE given by the acoustic peak measurements of the CMB anisotropies measured by the WMAP experiment.

The constraints on the simple parametrizations of DE are affected by the systematics, but the overall constraints are still strong even after their inclusion (see Figs. 4 and 6). More importantly, we found that systematic errors affect the constraints somewhat, reducing the w_0-w_a FoM by a factor of about 3 (see Table III), while the generalized

PC-based FoM is degraded by a factor of 3 to 4 (see Fig. 10). However, as the PC analysis shows, this degradation is mainly restricted to the first few numbers (PC amplitudes) describing DE. In fact, what is particularly impressive about the current data is that roughly five PCs are well constrained even in the presence of systematic errors (see Figs. 8 and 9).

In the spirit of testing for systematic effects in current data constraining DE, we also wondered if the relatively low detection significances of BAO features, ranging from about 2.4σ to 5.0σ in various surveys, change the overall cosmological constraints. While not a systematic error *per se*, the small but non-negligible probability that the BAO feature has not been detected in some of these surveys implies that the posterior probability of cosmological parameter values asymptotes to a small but nonzero value far from the likelihood peak [50]. We find that while the BAO-only constraints are somewhat affected, the combined constraints are not (see Fig. 11).

From all this, we conclude that current systematic errors do degrade DE constraints and FoMs, but not in a major way. Given that future constraints are forecasted to be much better, continued control of current systematic errors remains key for progress in characterizing DE.

[1] A. G. Riess *et al.*, Astron. J. **116**, 1009 (1998).
[2] S. Perlmutter *et al.*, Astrophys. J. **517**, 565 (1999).
[3] J. Frieman, M. Turner, and D. Huterer, Annu. Rev. Astron. Astrophys. **46**, 385 (2008).
[4] D. H. Weinberg, M. J. Mortonson, D. J. Eisenstein, C. Hirata, A. G. Riess *et al.*, arXiv:1201.2434.
[5] A. Conley, J. Guy, M. Sullivan, N. Regnault, P. Astier *et al.*, Astrophys. J. Suppl. Ser. **192**, 1 (2011).
[6] W. M. Wood-Vasey *et al.*, Astrophys. J. **666**, 694 (2007).
[7] M. Hicken, W. M. Wood-Vasey, S. Blondin, P. Challis, S. Jha, P. L. Kelly, A. Rest, and R. P. Kirshner, Astrophys. J. **700**, 1097 (2009).
[8] R. Kessler *et al.*, Astrophys. J. Suppl. Ser. **185**, 32 (2009).
[9] M. Sullivan, J. Guy, A. Conley, N. Regnault, P. Astier *et al.*, Astrophys. J. **737**, 102 (2011).
[10] T. M. Davis, E. Mortsell, J. Sollerman, A. Becker, S. Blondin *et al.*, Astrophys. J. **666**, 716 (2007).
[11] D. Rubin, E. Linder, M. Kowalski, G. Aldering, R. Amanullah *et al.*, Astrophys. J. **695**, 391 (2009).
[12] R. Amanullah, C. Lidman, D. Rubin, G. Aldering, P. Astier *et al.*, Astrophys. J. **716**, 712 (2010).
[13] N. Suzuki, D. Rubin, C. Lidman, G. Aldering, R. Amanullah *et al.*, Astrophys. J. **746**, 85 (2012).
[14] M. J. Mortonson, W. Hu, and D. Huterer, Phys. Rev. D **81**, 063007 (2010).
[15] M. Mortonson, W. Hu, and D. Huterer, Phys. Rev. D **82**, 063004 (2010).
[16] D. Huterer and A. Cooray, Phys. Rev. D **71**, 023506 (2005).
[17] Y. Wang and M. Tegmark, Phys. Rev. D **71**, 103513 (2005).
[18] C. Zunckel and R. Trotta, Mon. Not. R. Astron. Soc. **380**, 865 (2007).
[19] G.-B. Zhao, D. Huterer, and X. Zhang, Phys. Rev. D **77**, 121302 (2008).
[20] A. Hojjati, L. Pogosian, and G.-B. Zhao, J. Cosmol. Astropart. Phys. 04 (2010) 007.
[21] E. E. Ishida and R. S. de Souza, Astron. Astrophys. **527**, A49 (2011).
[22] A. Shafieloo, A. G. Kim, and E. V. Linder, Phys. Rev. D **85**, 123530 (2012).
[23] M. Seikel, C. Clarkson, and M. Smith, J. Cosmol. Astropart. Phys. 06 (2012) 036.
[24] G.-B. Zhao, R. G. Crittenden, L. Pogosian, and X. Zhang, arXiv:1207.3804 [Phys. Rev. Lett. (to be published)].
[25] J. Guy, P. Astier, S. Baumont, D. Hardin, R. Pain *et al.*, Astron. Astrophys. **466**, 11 (2007).
[26] B. C. Kelly, Astrophys. J. **665**, 1489 (2007).
[27] D. J. Eisenstein *et al.*, Astrophys. J. **633**, 560 (2005).
[28] F. Beutler, C. Blake, M. Colless, D. H. Jones, L. Staveley-Smith, L. Campbell, Q. Parker, W. Saunders, and F. Watson, Mon. Not. R. Astron. Soc. **416**, 3017 (2011).
[29] W. J. Percival *et al.* (SDSS Collaboration), Mon. Not. R. Astron. Soc. **401**, 2148 (2010).
[30] C. Blake, S. Brough, M. Colless, C. Contreras, W. Couch *et al.*, arXiv:1204.3674 [Mon. Not. R. Astron. Soc. (to be published)].
[31] C. Blake, E. Kazin, F. Beutler, T. Davis, D. Parkinson *et al.*, Mon. Not. R. Astron. Soc. **418**, 1707 (2011).
[32] A. G. Sanchez, C. Scoccola, A. Ross, W. Percival, M. Manera *et al.*, arXiv:1203.6616 [Mon. Not. R. Astron. Soc. (to be published)].
[33] L. Anderson, E. Aubourg, S. Bailey, D. Bizyaev, M. Blanton *et al.*, arXiv:1203.6594.
[34] J. A. Frieman, D. Huterer, E. V. Linder, and M. S. Turner, Phys. Rev. D **67**, 083505 (2003).
[35] E. Komatsu *et al.* (WMAP), Astrophys. J. Suppl. Ser. **192**, 18 (2011).
[36] N. Christensen, R. Meyer, L. Knox, and B. Luey, Classical Quantum Gravity **18**, 2677 (2001).
[37] J. Dunkley, M. Bucher, P. G. Ferreira, K. Moodley, and C. Skordis, Mon. Not. R. Astron. Soc. **356**, 925 (2005).
[38] N. Metropolis, A. Rosenbluth, M. Rosenbluth, A. Teller, and E. Teller, J. Chem. Phys. **21**, 1087 (1953).
[39] W. Hastings, Biometrika **57**, 97 (1970).
[40] A. Gelman and D. Rubin, Stat. Sci. **7**, 452 (1992).
[41] A. Lewis and S. Bridle, Phys. Rev. D **66**, 103511 (2002).
[42] http://cosmologist.info/cosmomc/.
[43] E. V. Linder, Phys. Rev. Lett. **90**, 091301 (2003).
[44] D. Huterer and G. Starkman, Phys. Rev. Lett. **90**, 031301 (2003).
[45] M. Chevallier and D. Polarski, Int. J. Mod. Phys. D **10**, 213 (2001).
[46] A. Albrecht *et al.*, arXiv:astro-ph/0609591.
[47] D. Huterer and M. S. Turner, Phys. Rev. D **64**, 123527 (2001).
[48] A. J. Albrecht *et al.*, arXiv:0901.0721.
[49] M. J. Mortonson, W. Hu, and D. Huterer, Phys. Rev. D **79**, 023004 (2009).
[50] B. A. Bassett and N. Afshordi, arXiv:1005.1664.
[51] R. Kessler, B. Bassett, P. Belov, V. Bhatnagar, H. Campbell *et al.*, Publ. Astron. Soc. Pac. **122**, 1415 (2010).
[52] R. Hlozek, M. Kunz, B. Bassett, M. Smith, J. Newling *et al.*, Astrophys. J. **752**, 79 (2012).